ELSEVIER

Polymer 43 (2002) 6101–6114

polymer

www.elsevier.com/locate/polymer

Covalent and non-covalently coupled polyester–inorganic composite materials

S.K. Young[a,1], G.C. Gemeinhardt[a], J.W. Sherman[a,2], R.F. Storey[a], K.A. Mauritz[a,*], D.A. Schiraldi[b], A. Polyakova[c], A. Hiltner[c], E. Baer[c]

[a]*Department of Polymer Science, The University of Southern Mississippi, Southern Station Box 10076, Hattiesburg, MS 39406-0076, USA*
[b]*KoSa, P.O. Box 5750, Spartanburg, SC 29304, USA*
[c]*Department of Macromolecular Science, Case Western Reserve University, University Circle, Cleveland, OH 44106, USA*

Received 27 December 2001; received in revised form 31 May 2002; accepted 22 July 2002

Abstract

Two types of organic/inorganic materials were synthesized via sol–gel reactions for tetraethylorthosilicate (TEOS) and organo-alkoxsilane monomers in the presence of poly(ε-caprolactone) (PCL): (1) non-covalent hybrids, in which PCL and silicate, and PCL and organically modified silicate (ORMOSIL), phases are coupled by non-bonded interactions; (2) covalent hybrids in which triethoxysilane–telechelic PCL molecules form chemical bonds with a sol–gel-derived silicate phase. Chemical structures were verified using FTIR and ^{13}C NMR spectroscopies and MALDI-TOF mass spectrometry. The constant PCL phase T_g for the silicate–PCL hybrids of (1) implies poor organic/inorganic mixing, but dual-melting endotherms varied with silicate content. TGA revealed significant elevation of degradation onset temperature (T_d) of (1) and suppression of the low temperature chain scission process. No PCL glass transition is seen for ORMOSIL–PCL hybrids where diethoxydimethylsilane is the co-monomer and melting occurs in one step, and there are significant increases in T_d. Likewise, no glass transition is seen when acetoxypropyltrimethoxylsilane is the semi-organic co-monomer, but there are dual-melting endotherms. Triethoxysilane-endcapped PCL was synthesized and its microstructure verified by GPC, MALDI-TOF mass spectrometry, FTIR and NMR spectroscopies. T_g for this telechelic PCL that was reacted with a small fraction of TEOS increases relative to hydroxy-telechelic PCL due to formation of phase-linking Si–O–Si bonds through end groups. The temperature/magnitude of the melting transition decreased upon inorganic modification. TGA showed appreciable increase in T_d relative to PCL and both the high and low temperature degradation processes were hindered. Silane–telechelic PCL films have oxygen permeability values less than that of pure PCL, which is totally attributed to a decrease in diffusion coefficient. © 2002 Published by Elsevier Science Ltd.

Keywords: Silane–telechelic poly(ε-caprolactone); Sol–gel process; Organic–inorganic hybrids

1. Introduction

Sol–gel processes for metal alkoxides and organo-alkoxysilanes have been used to form porous monolithic structures, porous, high surface/volume gel particles, filler particles for the mechanical reinforcement of polymers, optical fibers, and coatings and surface treatments that impart corrosion resistance to metals or scratch resistance to polymers [1–3]. A beneficial feature of this process is that it occurs at low temperatures as opposed to the extremely high temperatures required in conventional inorganic glass formation. The underlying hydrolysis and condensation reactions, gel growth and resultant solid structures have been discussed in several reviews [1,4].

Numerous silica-based sol–gel systems have been examined in the literature, involving organic–inorganic monomers [2,5,6], organic–inorganic associations [7–10], organic–inorganic interpenetrating networks [5,10,11], and organic–inorganic telechelic polymers [12,13]. A recent compendium of papers describing a diverse collection of organic/inorganic nanocomposite systems includes reports of materials derived via sol–gel processes [14]. The two types of materials of interest here are non-covalent organic/inorganic composites, and covalent composites based on

* Corresponding author. Tel.: +1-601-266-5595; fax: +1-601-266-5635.
E-mail address: kenneth.mauritz@usm.edu (K.A. Mauritz).
[1] Present address: US Army Research Laboratory, WMRD-Polymers Branch, Attn: AMSRL-WM-MA/Bldg 4600, APG, MD 21005-5069, USA.
[2] Present address: The Dow Chemical Company, Corporate R&D, B1215, 2301 Brazosport Blvd., Freeport, TX 77541-3257B-1215, USA.

0032-3861/02/$ - see front matter © 2002 Published by Elsevier Science Ltd.
PII: S0032-3861(02)00515-3

telechelic organic polymers. Here, 'non-covalent' refers to hybrid materials in which the interactions between the organic and inorganic phases consist of non-bonded interactions due to van der Waals, electrostatic and hydrogen bonding forces. These types of composites were considered in this work within the context of increasing the thermal and mechanical properties of the base polymer, which is poly(ε-caprolactone) (PCL). Conventional organic–inorganic (filler) composites can have problems with particle agglomeration that occurs during the physical mixing-in of pre-formed inorganic particles and ways are sought to promote good particle dispersion. Non-covalent composite formation based on sol–gel chemistry often focuses on the use of organically modified silicates (ORMOSILs) that contain chemical moieties similar to those on the polymer backbone to increase compatibility, that is, decrease interfacial surface tension. While covalent composites also use this batch synthesis concept, they additionally rely on the covalent bonds between the two systems to increase phase coupling. It should be mentioned that our distinction between 'non-covalent' and 'covalent' hybrids corresponds to the 'class I' and 'class II', respectively, categories of Sanchez and Ribot [15].

Landry and coworkers [7] investigated the use of copolymers consisting of monomers capable of interacting with a growing inorganic network. Organic–inorganic non-covalent composites, where the polymer is polystyrene, poly(vinyl methyl ether), or poly(styrene-*co*-acrylonitrile), were developed utilizing sol–gel reactions for titanium isopropoxide. A copolymer of polystyrene and polyvinyl phenol was used as a compatibilizing agent in every synthesis batch. By including moieties that would strongly interact with the inorganic phase (i.e. –OH groups) and have a similarity to the organic phase, the copolymer interfacial tension might be viewed as being reduced via hydrogen bonding and polar interactions.

Along these same lines, Novak and coworkers [10] investigated the effect of synthesis of pseudo-simultaneous interpenetrating polymer networks (sIPNs), where the formation of both an organic polymer and an inorganic glass network would occur synchronously, on material properties. 2-Trimethylsiloxyethylmethacrylate and 2-trimethylsiloxyethylacrylate were individually polymerized with tetraethylorthosilicate (TEOS). By forming the materials in situ, the alcohol liberated from the formation of the inorganic network (2-hydroxyethyl methacrylate or 2-hydroxyethylacrylate) is used directly in the organic polymerization. Thermal analysis of the films showed an increase in the polymer T_g with glass loadings as low as 10% by weight. The existence of a well-mixed system, with the presence of strong interfacial interactions was supported by ^{13}C NMR spectroscopic studies that showed a shift in the resonance of the carbon adjacent to the hydroxyl group when the oxygen is covalently bound to the silicon atom. Analysis by dynamic mechanical analysis also showed an increase in T_g and a disappearance in the tan δ peak, indicating significant chain mobility reduction, which, in turn, increased the use temperature of the polymer by about 100 °C.

While there are many ways to covalently incorporate polymerizable inorganic monomers into a polymer, in this work, the specific interest is in telechelic materials. A telechelic polymer contains one or more functional, often reactive, end groups with which selective covalent bonds can be formed with other molecules. Schmidt and Phillip [16] investigated the benefits of incorporating acrylic polymers, containing monomer units with alkoxysilane functionality, in epoxysilane and titanium-alkoxides for use as contact lens materials. These materials, in the absence of the acrylic polymer, had poor mechanical properties and increased brittleness. In order to achieve the desired properties, a copolymer of methyl methacrylate, hydroxyethyl acrylate, and methacryloxypropyltrimethoxysilane were incorporated to act as linear crosslinking elements. The tensile strength was improved by 40% with the modulus of elasticity remaining unchanged. The flexibility improved greatly while the hardness and refractive index slightly decreased. These mechanical properties were all optimized without sacrificing wettability of the final material or O_2 permeability.

Wilkes et al. [17–19] and Mark and Sur [20] developed hybrid materials, termed 'ceramers', that were derived via condensation reactions between TEOS and triethoxysilane- and silanol–telechelic polydimethylsiloxane chains. Wilkes et al. [21] also developed hybrids based on sol–gel reactions of TEOS in the presence of triethoxysilane–telechelic poly(tetramethylene oxide).

Tian et al. [13,22] studied the properties of PCL ceramers for possible use as coatings for bone implants and prosthetic devices and as supports for enzyme immobilization. TEM analysis showed some degree of co-continuity between the two phases when the composition was 50/50 (PCL/SiO_2). Also studied was the effect of varying the ethanol content, as well as varying the polymer-to-alkoxysilane ratio, on the final appearance of the films. The gelation time was observed to be independent of the PCL content, but the final appearance of the films was related to the amount of PCL and ethanol in the system. An increase in the amount of ethanol and a decrease in the amount of PCL lead to an increase in the optical clarity of the films.

With regard to thermal stability, Persenaire et al. [23] examined the degradation of PCL using coupled high resolution thermal gravimetric analysis (TGA), mass spectrometry and FTIR analyses. TGA scans showed a main degradation event having an inflection point at 420 °C and a shoulder at ~360 °C. The underlying mechanism for the low temperature event consists of random chain scission that occurs by ester pyrolysis along the entire chain. The unzipping of chains accounts for the high temperature event and this proceeds by a backbiting reaction from the hydroxyl end group onto the ester function of the last monomeric unit and ε-caprolactone cyclic monomers are

formed. Hydroxyl end groups are required for this reaction and, when hydroxyl groups were acetylated, depolymerization was limited and there is an enhancement in the contribution of the first step (which can generate water that can cause hydrolysis). Thus, it would seem that conversion of PCL to a telechelic form would enhance thermal stability by eliminating terminal hydroxyl groups. This is one of the synthetic modifications that will be described below.

With regard to environmental stability, PCL can be slowly hydrolyzed but is more biodegradable [24–28] in the presence of microbes found in soil, and in vivo [29]. Chain cleavage is known to proceed in the amorphous regions of this semi-crystalline polymer [30]. Molecular weight and its distribution, as well as crystallinity, significantly affect PCL biodegradation rates. The PCL T_g is around -60 °C, T_m usually occurs at around 55–65 °C and thermal decomposition temperature is around 250 °C [31]. PCL is tough, but one of its negative attributes is its low melting point, which can compromise mechanical properties at elevated use temperatures. Thus, it is of great interest to elevate T_m or suppress the degree of melting.

Mauritz et al. [32,33] successfully incorporated silicate and ORMOSIL nanostructures in polymer sol–gel reaction matrices. Fluorescence probe and liquid uptake studies have shown that the microenvironment within Nafion®/ORMOSIL nanocomposites can be tailored with regard to polarity and hydrophobicity [34]. The mechanical tensile and dynamic mechanical properties of Nafion® can also be modified in this way [35]. In other studies, the phase-separated morphologies of styrene-containing hard/soft block copolymers have been demonstrated to act as templates for the in situ, domain-targeted, sol–gel polymerizations of TEOS [36].

The main focus of the work reported here is the creation of inorganically modified polyesters that could serve as biodegradable packaging materials that will have enhanced thermal stability by virtue of elevated T_m. The goal was to synthesize both non-covalent and covalent PCL hybrids based on polymer in situ sol–gel reactions for TEOS and organo-alkoxysilanes. The resultant composites were examined for low magnification surface morphology as well and the thermal properties determined. Homogeneous samples that were good film formers and possessed good thermal properties were then analyzed for oxygen permeation to assess the influence of the inorganic inclusions on polymer chain mobility as it affects molecular transport.

2. Experimental

2.1. Materials

3-Isocyanatopropyltriethoxysilane (ICPTES), TEOS, diethoxydimethylsilane (DEDMS), 99.8% anhydrous ethylene glycol, diethylene glycol, 1,4-diazabicyclo[2.2.2]octane (DABCO), tetrahydrofuran (THF) and deuterated chloroform were purchased from Aldrich Chemical Company and used as received. Ethanol (95%, EtOH) was purchased from Aaper Chemical Company. Methylene chloride, hydrochloric acid (HCl), and hexanes were purchased from Fisher Chemical Company. 95% Stannous (2-ethylhexanoate) was purchased from Sigma Chemical Company and used as received. Acetoxypropyltrimethoxysilane (APTMS) was purchased from Gelest, Inc. The ε-caprolactone (TONE® ECHP) monomer was supplied by Union Carbide. All water used was distilled and deionized.

2.2. Synthesis of hydroxy-telechelic poly(ε-caprolactone)

Three low-molecular weight (2000, 4000, and 12,000 g/mol) hydroxy-telechelic PCL polymers were synthesized by the ring-opening polymerization of ε-caprolactone using a diol, ethylene glycol, as the initiator and stannous(2-ethyl hexanoate) as the catalyst (1.4×10^{-4} mol catalyst/mol monomer) [37]. Molecular weights were determined using gel permeation chromatography (GPC) calibrated with polystyrene standards. All polymerizations were conducted in the bulk under a nitrogen blanket at 135 °C. Glassware was dried overnight in a 200 °C oven. A typical experimental procedure was as follows: a 100 ml round-bottom flask was charged with 2.5×10^{-2} g (1.4×10^{-4} mol catalyst/mol monomer) of stannous octoate, 2.16 g (2.03×10^{-2} mol) of diethylene glycol and 50.1 g (4.38×10^{-1} mol) ε-caprolactone. The flask was then equipped with a Chesapeake-style mechanical stirrer with a Teflon® stirrer blade and immersed in a constant temperature oil bath. The polymerization was allowed to proceed for 10 h at 135 °C, after which the flask was removed from the oil bath and allowed to slowly cool to room temperature. The resulting polymer was dissolved in 200 ml (25%, w/v) of methylene chloride and precipitated by combining the solution with a 10× excess of vigorously stirred hexanes. The hexanes were decanted off and the resulting solid polymer was washed twice with 200 ml of hexanes. The polymer was re-dissolved in methylene chloride and the precipitation process was repeated. The resulting catalyst and monomer free polymer was dried at room temperature in vacuo for at least 1 week before utilizing it in thin films.

Low molecular weight polymers were used in these experiments so that end group modifications could be detected by spectroscopic means. Of course, mechanical properties, especially toughness, are compromised in this way and the hybrids based on these low molecular weight polymers are considered as model systems.

2.3. Film formation: bulk TEOS

Bulk TEOS films were prepared by mixing TEOS, H_2O, and ethanol, as a co-solvent, in an aluminum petri dish. Mixtures were made such that H_2O/TEOS = 4:1 (mol/mol),

and $H_2O/EtOH = 1:1$ (mol/mol). The petri dish was covered with perforated Parafilm® to slow the evaporation/gelation process. After gelation, the films were placed in a vacuum oven at 50 °C/30 Torr for 2 days to ensure complete solvent evaporation.

2.4. Non-covalent film formation: TEOS/PCL hybrids

Non-covalent films of PCL ($M_w = 4000$ g/mol) with in situ-grown silicate phases were prepared by combining a mixture of the polymer dissolved in THF and TEOS monomer. The TEOS/PCL compositions were prepared based on a total mass of TEOS + polymer at varying weight ratios. The ratios of TEOS/PCL that were prepared varied from 90:10 to 10:90 wt%. The mole ratio of water-to-silicon alkoxide group was always set at 1:1. A catalytic amount of HCl (0.1 M) was added to the mixture to initiate the sol–gel reaction and the solution was mixed in a beaker until it appeared homogeneous. Then, the solution was placed in a glass evaporating dish and covered with perforated Parafilm® to slow the evaporation/gelation process. After gelation, the films were placed in a vacuum oven at 50 °C/30 Torr for 2 days to ensure complete solvent evaporation. On visual inspection, it was seen that the most optically uniform films corresponded to TEOS/PCL ratios between 80:20 and 70:30.

2.5. Non-covalent film formation: (TEOS/co-reactant) ORMOSIL/PCL hybrids

Non-covalent films of PCL with in situ-grown ORMOSIL phases were prepared by combining a mixture of the polymer dissolved in THF and TEOS/semi-organic co-monomers. DEDMS and APTMS were used as the semi-organic co-monomers. The polymer was incorporated at 25 wt% of the total weight of the silanes. The TEOS/co-reactant mole ratios were 1:0, 2:1, 1:1, 1:2 and 0:1 while the H_2O/Si alkoxide group mole ratio was always 1:1. A catalytic amount of HCl (0.1 M) was added to the polymer/inorganic mixture to initiate the sol–gel reaction. The solution was mixed in a beaker and placed in a glass evaporating dish which was subsequently covered with perforated Parafilm® for controlled drying. After the solution gelled, the films were placed in a vacuum oven at 50 °C/30 Torr for 2 days to ensure complete solvent evaporation.

2.6. Synthesis of silane-endcapped telechelic poly(ε-caprolactone)

The endcapping reaction was performed on polymers of three different low molecular weights (2000, 4000, and 12,000 g/mol). A three-necked round-bottom flask was equipped with a magnetic stir bar, thermometer, West condenser, and a nitrogen inlet/outlet. To this flask was added the solvent (toluene), ε-caprolactone, ICPTES, and the catalyst (DABCO). Five gram of PCL was used in all reactions. The PCL/ICPTES mole ratio was set at 1:2 to achieve an equal stoichiometry of reactive groups. The catalyst was added at 1 equiv. This procedure was modeled after that of Tian and coworkers [13].

2.7. Silane–telechelic poly(ε-caprolactone) film formation

After the triethoxysilane functionalization of the PCL end groups, the product was dissolved in methylene chloride, 5% TEOS was added, and the solution was cast in an evaporating dish and then left exposed to atmospheric conditions. Within 3 h, exposure to atmospheric moisture resulted in a crosslinked film of pure telechelic polymer with 5% reacted TEOS. The film was removed from the evaporating dish and tested accordingly.

2.8. Gel permeation chromatography

GPC was used to determine average molecular weight, molecular weight distribution, and the polydispersity index (PDI) $= M_w/M_n$, of polymer samples with respect to polystyrene standards (Polysciences, Inc.). The GPC system configuration has been described previously [38].

2.9. Matrix assisted laser desorption/ionization time-of-flight mass spectrometry (MALDI-TOF MS)

A PerSeptive Biosystems Voyager-RP MALDI-TOF Biospectrometry Workstation equipped with 1 m vertical flight tube, tunable two-stage ion source, nitrogen laser operating at 337 nm with a 3 ns pulse delay, dual differential turbomolecular pump for ultra-high vacuum, and positive ion detection was used to analyze both hydroxy-telechelic PCL and silane–telechelic PCL. All samples were dissolved in THF, freshly distilled from CaH_2, to a final concentration of 8 mg/ml. Separately, a THF solution of 2,5-dihydroxybenzoic acid (DHBA) (40 mg/ml), used as matrix material, was prepared. A 1.5 μl sample of a 1:1 mixture of polymer/matrix solution was applied to a polished gold target plate and allowed to air dry immediately before analysis. Each MALDI spectrum was the average of 256 laser shots.

2.10. FTIR spectroscopy

In the same way as that for the MALDI-TOF MS experiments, samples were dissolved in THF, placed dropwise onto NaCl crystals, and allowed to dry in order to have thin films. Spectra were obtained using a Bruker IFS 88 Spectrometer over a range of 400–4000 cm^{-1}. The number of sample scans and resolution were 200 and 4 cm^{-1}, respectively. All spectra were evaluated utilizing the GRAMS/32 Spectral Notebase™ software version 5.05. FTIR spectroscopy can be used to verify the presence of specific molecules and bond formation. Several references

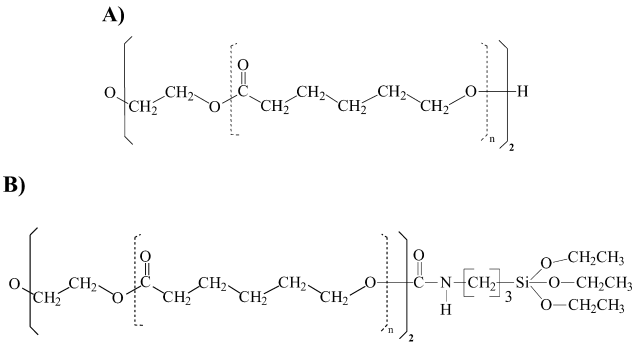

Fig. 1. Chemical structures of (A) hydroxy- and (B) triethoxysilane–telechelic PCL.

assign details for spectra [39–41], which contain bands that are characteristic of silicate materials and silicate phases incorporated into organic materials.

2.11. ^{13}C NMR spectroscopy

^{13}C NMR spectra were obtained on a Bruker AC-200 spectrometer using 5 mm o.d. tubes, deuterated solvents, and tetramethylsilane as an internal reference. For ^{13}C NMR spectra, sample concentrations were approximately 25% (w/v). All NMR spectra were evaluated utilizing the GRAMS/32 Spectral Notebase™ software version 5.05. NMR spectra yield quantitative structural information and can be used to determine the precise structure of the monomer or polymer.

2.12. Thermal gravimetric analysis

Experiments were conducted using a Mettler thermal analysis workstation. TGA experiments were carried out under nitrogen using a Mettler TGA850 thermal analyzer. The temperature was increased (one scan) from 25 to 800 °C at 20 °C/min. Degradation temperatures, T_d, are reported as the onset of degradation as calculated from the intersection of the baseline of 100% sample mass and the line tangent to the inflection point. Sample masses were approximately 10–20 mg.

2.13. Differential scanning calorimetry (DSC)

Experiments were conducted using a Mettler thermal analysis workstation. DSC data were collected with a DSC 30 and TC 15 controller. Dry samples, of mass 5–10 mg, were prepared in aluminum oxide pans and sealed. First and second heating scans were run from −100 to 100 °C at 10 °C/min with a nitrogen purge. The polymer glass transition and polymer melting endotherms were probed using this method. The polymer T_g is reported here as the temperature at the inflection point that appears on the 2nd scan. The DSC plots were normalized to the amount of polymer in each film. This was determined by calculating the mass loss from the TGA experiment, which is approximately equal to the amount of polymer in the film.

2.14. Environmental scanning electron microscopy (ESEM)

An Electroscan E-20 Environmental Scanning Electron Microscope was utilized in collecting data. These studies were used to examine the external film surfaces and to probe heterogeneous microstructure in the films.

2.15. Oxygen transport measurements

Plaques of the polymers were compression molded according to an earlier reported method [42]. Test specimens were cut from the plaques, mounted, and the oxygen flux at 25 °C, 0% relative humidity, and 1 atm pressure was measured with a MOCON OX-TRAN 2/20 instrument. The diffusivity (D) and permeability (P) values for each test were obtained by fitting the flux-time curve to the solution of Fick's second law. The error in determining the two fitting parameters, P/l and D/l^2, where l is the membrane thickness, was estimated at less than 2% [42–44]. Improvements in sample preparation and masking techniques have resulted in this degree of permeation measurement accuracy that is greater than that possible through the common specified usage of this commercial instrument. A stock polymer is kept on hand, tested periodically, and has been observed to yield the same permeation value reproducibly to within 2% over the course of several experiments. Each material was tested in duplicate and the average values are those that are reported.

3. Results and discussion

3.1. Synthesis of hydroxy-telechelic poly(ε-caprolactone)

The chemical structure for PCL is shown in Fig. 1A. The synthesis of the hydroxy-endcapped telechelic polymer produced a fine white powder that can be cast into films whose surface morphology, on the scale of tens-of-microns, consists of a rough texture. The polymer was observed to be soluble in typical polar organic solvents (acetone, methylene chloride, chloroform, toluene, THF, and DMF), but was not soluble in hexane. The MALDI-TOF MS spectrum, seen in Fig. 2, of the hydroxy-telechelic PCL, shows a peak-to-peak spacing of 114, which is the molecular weight of the monomer repeat unit. There are several other small peaks in the spectrum, which will not be discussed because they have been reported in a previous paper [45]. The data gives an average molecular weight of 4234 g/mol and PDI = 1.4, which corresponds well with the GPC data (M_n = 3367, M_w = 4780, PDI = 1.42), which will not be shown here.

The FTIR spectrum for hydroxy-telechelic PCL, seen in Fig. 3, contains bands that are characteristic of this polymer. These bands include the methyl C–H stretch at 2850 and

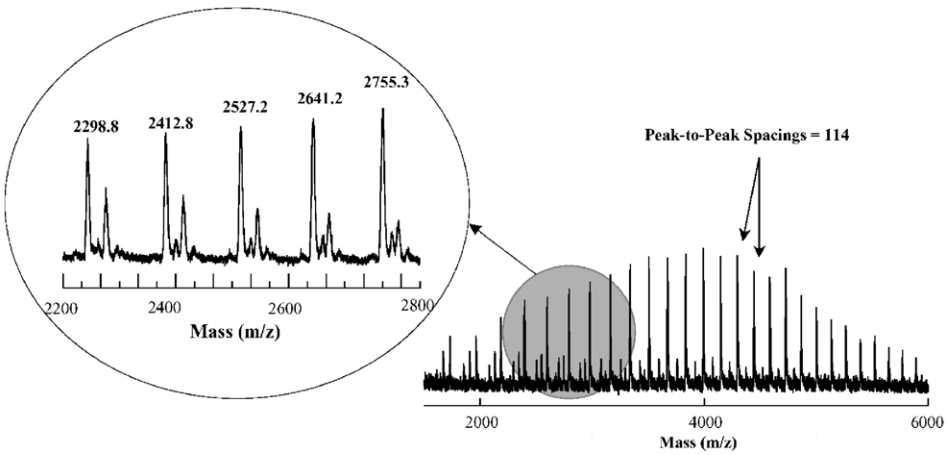

Fig. 2. MALDI-TOF MS spectrum of hydroxy-telechelic PCL.

2900 cm^{-1}, the carboxylic (C=O) stretch at 1730 cm^{-1}, and the C–(C=O)–O stretch that is common to esters at 1250 cm^{-1}.

The ^{13}C NMR spectrum of PCL is shown in Fig. 4. There are three peaks in the carbonyl region designated 1, 1^{EG}, and 1^{OH}. The largest peak (1) located at 173.5 ppm is attributed to the main chain ester carbonyl carbon atoms derived from internal ε-caprolactone repeat units that were adjacent to other caprolactone units. The main chain resonance (1) was flanked on the downfield side by 1^{OH} and on the upfield side by 1^{EG} located at 173.6 and 173.1 ppm, respectively. Peak 1^{EG} was attributed to carbonyl carbons adjacent to the initiating ethylene glycol fragment while peak 1^{OH} was attributed to carbonyl carbons of terminal PCL telechelic hydroxy-endcapped units bearing hydroxyl end groups. The methylene carbons of the PCL repeat units were defined as α, β, γ, δ, and ε, in order of increasing distance from the carbonyl carbon starting with the closest, α. Main chain ε-caprolactone methylene carbons, α, β, γ, δ and ε were assigned to resonances located at 34.1, 25.3, 24.5, 28.3, and 64.3 ppm, respectively. The smaller peak downfield from δ at 32.3 ppm (δ^{OH}) was assigned to δ-carbons of terminal hydroxy-functional PCL units.

3.2. Non-covalent film formation: TEOS–PCL hybrids

The gelation times of the successful films were independent of the concentration of polymer in the formulation for the particular cases studied. In all cases, approximately 3 days were required for complete film formation. After drying in a vacuum oven, as described, the films were removed and analyzed. While every film appeared somewhat opaque, an increase in clarity with decreasing polymer content was observed. All of the films were fracture-prone but demonstrated a decrease in brittleness as the polymer fraction increased. ESEM micrographs were taken of several different film surfaces. PCL of low molecular weight is highly crystalline and tends to form brittle films. A characteristic film of pure silica derived via sol–gel reactions for TEOS was seen to be brittle as demonstrated by distinctive cracks that are characteristic of an inorganic oxide glass. On the other hand, the TEOS–PCL hybrid film does not show this cracking. While the TEOS–PCL film surface is not smooth, there is a definite decrease in roughness relative to the pure polymer film surface. The film has an optical appearance that is uniform in texture, possibly indicating that the polymer was homogeneously distributed throughout this hybrid material.

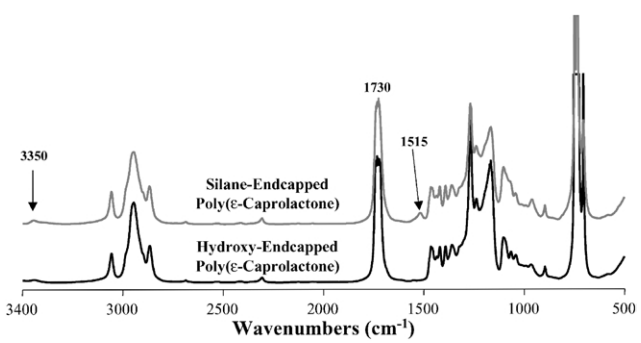

Fig. 3. FTIR spectra of hydroxy- and triethoxysilane-endcapped PCL.

TGA and DSC analyses of the PCL/silicate films were conducted in order to determine the effect of the inorganic incorporation on T_d, T_g and the melting temperature, T_m, of the PCL component. It is the latter number as well as the degree of crystallinity that determines the upper use temperature in terms of mechanical properties. The DSC and TGA plots that are displayed represent only half of the samples that were analyzed in the interest of brevity, although the same general trend is followed by all data.

The DSC 2nd heating scans for the PCL control and series of PCL/silicate non-covalent hybrids are shown in Fig. 5. The total scan has been divided into a low temperature region to show the PCL glass transition and a high temperature region around the melting transition. No other transitions are present. For these materials, a slight inflection is observed in the temperature range −70 to −60 °C, which is in the region of the glass transition reported for PCL [31]. T_g values for the hybrids and pure

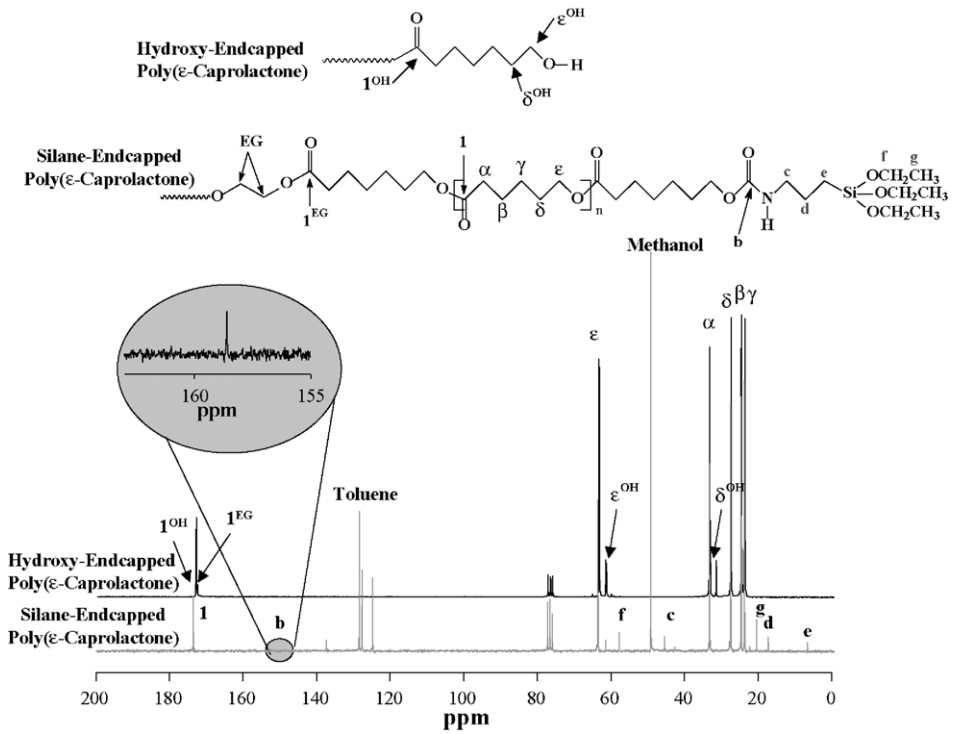

Fig. 4. Structure and ^{13}C NMR spectrum of hydroxy- and triethoxysilane-endcapped PCL.

PCL control are listed in Table 1. The rather constant value of T_g implies poor organic/inorganic component mixing as PCL chain segmental mobility is not significantly affected by this inorganic modification. It is reasonable to expect that the 1st heating provided thermal kinetic energy to drive condensation reactions between SiOH groups in the inorganic phase to further completion, but that the PCL chains did not become trapped in silicate structures that became more interconnected by Si–O–Si bonds.

In contrast, the nature of the PCL melting endotherms did vary with silicate content and consist of dual peaks. Dual-melting endotherms have been reported for other polymers, including poly[ethylene terephthalate (PET)] and poly-[ethylene-*ran*-methacrylic acid] and ionomer forms (Surlyn®)]. The shape of these peaks depends on thermal history and temperature scanning rate. This phenomenon, which is not entirely understood, has been variously attributed to the melting of two crystal structures that existed in the sample before heating or to partial melting of pre-existing crystallites, followed by re-crystallization and then melting. More directly related to the work reported here, sol–gel-derived [Surlyn®-Zn^{2+}]/silicate [46] and [PET ionomer]/silicate [47] hybrids also were seen to exhibit dual-melting.

Table 1
Thermal analysis data for TEOS–PCL films

TEOS/PCL (mol/mol)	T_g (°C)	$T_{m1}^{min}/T_{m2}^{min}$ (°C)	T_d onset/midpoint (°C)
90:10	~ −63.3	46.7, 50.2	416/429
80:20	–	–	414/430
70:30	~ −63.8	49.5	415/428
60:40	–	–	412/430
50:50	~ −63.6	~46.8, 51.2	413/430
40:60	–	–	416/430
30:70	~ −63.1	~47.0, 51.3	415/430
20:80	–	–	413/430
10:90	~ −62.2	47.8, 49.3	404/430
Pure PCL	−63.0	46.7, 50.2	300/387

Values for the temperature-at-minimum for the curves shown in Fig. 5 are listed in Table 1. T_{m1}^{min} and T_{m2}^{min} refer to the high and low temperature peaks, respectively. Owing to the fact that the peaks overlap so that one melting event is superimposed on the other, as well as the fact that some peaks are only visible as a shoulder on the major peak, T_{m1}^{min} and T_{m2}^{min} should be viewed as semi-quantitative markers of these transitions. There is no appreciable difference in the position of peak 1 or 2 with hybrid composition although there is a difference in their relative magnitudes in this series of hybrid compositions. Interestingly, the peaks are best resolved and have practically the same positions for the pure PCL and 90:10 hybrid. Given that all samples experienced the same thermal history, it is possible that the silicate inclusions interacted with the crystalline regions in PCL to account for the peak magnitude differences.

Also, it can be seen on comparing the vertical scales of the top and bottom graphs in Fig. 5 that the glass transition is a considerably less-profound event than the melting transition.

The TGA scans for these same materials are shown in Fig. 6 and T_d values are listed in Table 1. First, it is seen that degradation occurs in the two steps as described by

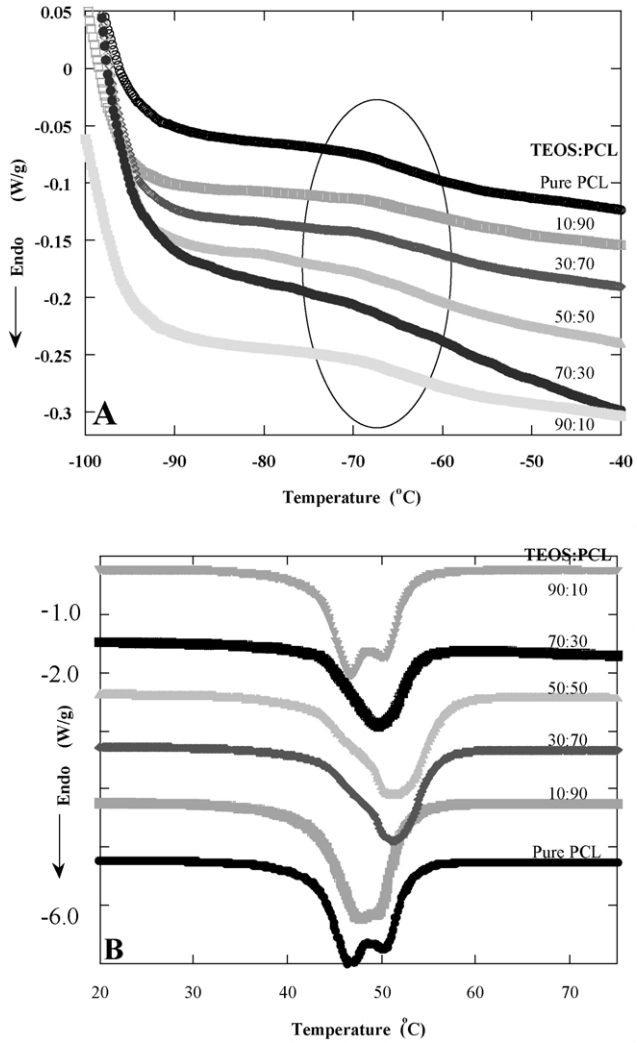

Fig. 5. DSC second heating scans for TEOS–PCL films showing (A) glass transition and (B) melting temperature ranges. Plots are vertically offset for clarity of viewing.

Persenaire et al. [23]. Incorporation of a silicate component within PCL clearly retards the onset of thermal degradation and the two-step nature disappears. T_d (onset) for the TEOS/PCL = 10:90 hybrid, the major composition of which is PCL, is 104 °C higher than that for pure PCL. T_d (onset and midpoint) is even higher for the other hybrids, but is essentially invariant with respect to the TEOS/PCL ratio. It might be concluded that the presence of silicate structures more strongly inhibits the first degradation step that involves statistical chain scission. The 90:10 hybrid is mainly silica and the early weight loss seen on the TGA scan might be due to the loss of water and solvent, some of which might be generated by thermally driven condensation reactions between unreacted SiOH groups.

3.3. Non-covalent film formation: ORMOSIL–PCL hybrids

TEOS/DEDMS–PCL films were successfully synthesized. ESEM shows that a film having a 2:1 ORMOSIL composition has a considerably smoother surface as compared with the surfaces of pure PCL and TEOS/PCL films, although there can be indentations as well particulate features on the surfaces. All TEOS/DEDMS–PCL films showed surface cracks similar to those seen for the pure SiO_2 film. As DEDMS content increased, the ability to form films diminished, presumably due to increasingly fewer SiO_4 crosslink junctions generated by hydrolyzed TEOS molecules. In fact, the pure DEDMS film (TEOS/DEDMS = 0:1) did not gel and remained in a liquid state. Others have noted a similar absence of long range polymerization of DEDMS in bulk systems [48]. Dimethylsiloxane oligomer rings are known to form in this way and these were also detected by ^{29}Si SS NMR spectroscopy by Deng and Mauritz in Nafion® membranes after in situ hydrolysis–condensation reactions of DEDMS [49]. Also noted by Mackenzie et al. and observed in this work was a marginal increase in the optical clarity of the films as DEDMS content increased. Perhaps this is due to an increase in the organic character of the silicate phase, which would enhance organic–inorganic phase compatibility. The films were hard and brittle at high TEOS concentrations but are softer and a waxier feel was experienced with increasing DEDMS content. This again can be attributed to an increase in the organic content and a reduction in the molecular connectivity of the ORMOSIL phase as well as reduction in macromolecular entanglements that might otherwise provide material cohesion and toughness.

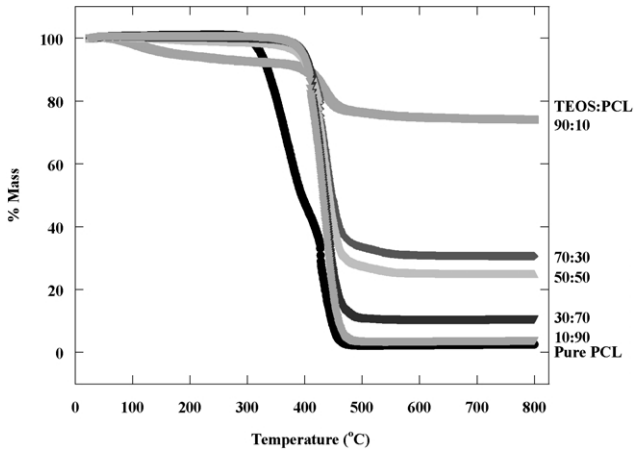

Fig. 6. TGA scans for TEOS–PCL films.

DSC scans for the TEOS/DEDMS–PCL films are shown in Fig. 7. There is no evidence for a glass transition at any of the ORMOSIL compositions. In contrast with the behavior seen in Fig. 5, melting in the presence of incorporated ORMOSIL structures is not of a two-step nature and, excepting the 1:2 composition, the single peak lies closer to the high temperature peak for unfilled PCL. T_m^{min} values, listed in Table 2, increase slightly with increasing TEOS fraction and the area under the melting peaks for the hybrids is less than that for pure PCL.

TGA scans for these films are shown in Fig. 8 and values

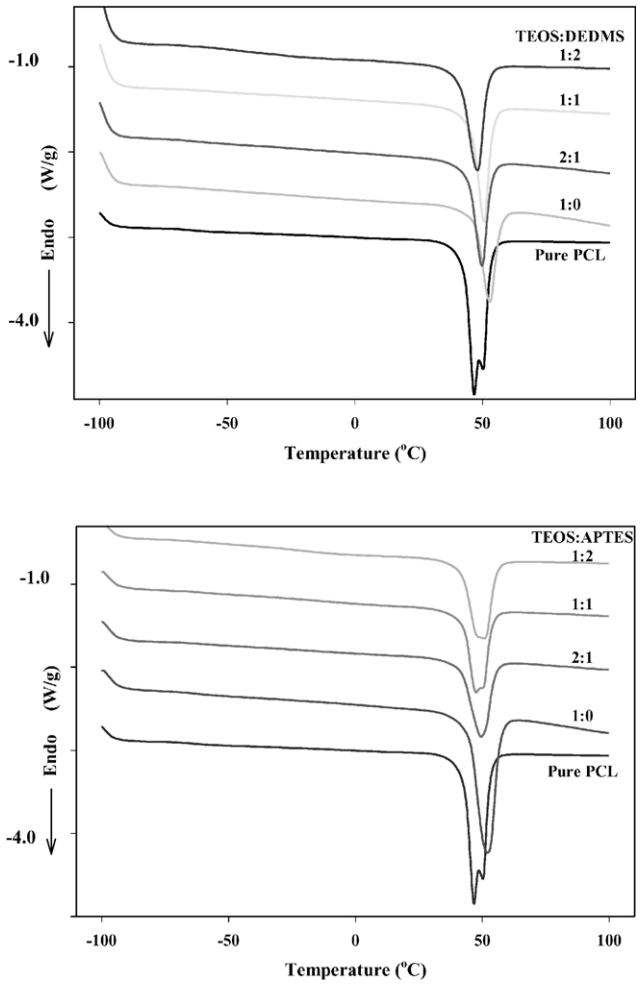

Fig. 7. DSC 2nd heating scans of TEOS/DEDMS–PCL (top) and TEOS/APTMS–PCL (bottom) hybrid films. The curves are vertically offset for viewing clarity and are all drawn to the same scale.

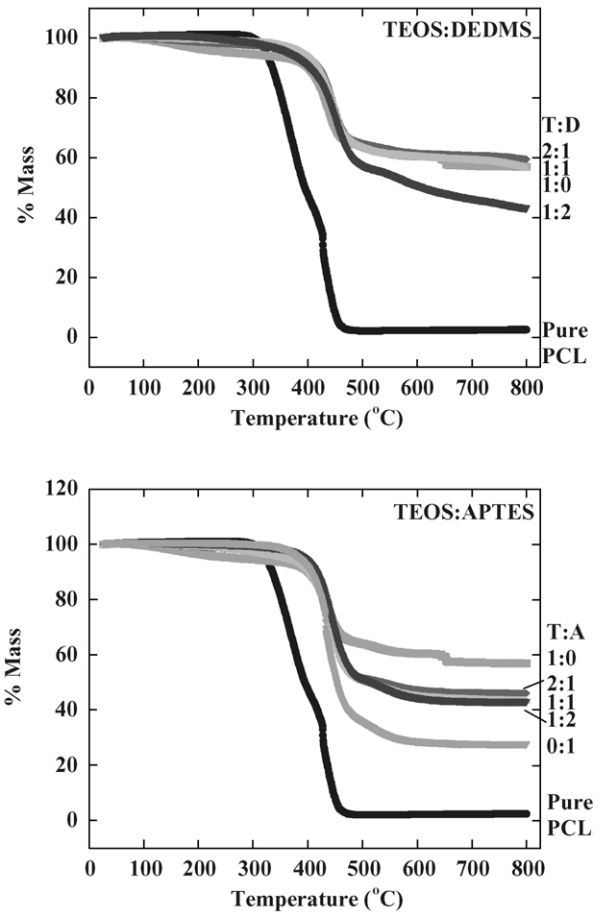

Fig. 8. TGA scans of TEOS/DEDMS–PCL (top) and TEOS/APTMS–PCL (bottom) hybrid films.

for T_d are listed in Table 2. There are substantial increases in T_d relative to pure PCL in the range $\Delta T_d(\text{onset}) = 103–109$ °C, although values for the hybrids do not differ greatly from one another. The relative mass of organic component that was thermally degraded was not as great as that for the TEOS–PCL films. As for TEOS-modified PCL, the TGA degradation profile is no longer of a two-step nature and the degradation onset occurs at an approximate temperature as that for the second step for unmodified PCL. Again, it is possible that this ORMOSIL modification inhibits the first degradation step that involves statistical chain scission.

Table 2
Thermal analysis data for (TEOS/DEDMS)–PCL and (TEOS/APTMS)–PCL hybrid films

Sample	TEOS/DEDMS–PCL		TEOS/APTES–PCL	
	T_{m1}/T_{m2} (°C)	T_d onset/ midpoint (°C)	T_{m1}/T_{m2} (°C)	T_d onset/ midpoint (°C)
Pure PCL	46.7, 50.2	300/387	–	–
1:0	52.8	406/433	52.0	406/433
2:1	49.7	409/435	49.5	409/435
1:1	50.5	406/435	47.5, 50.2	405/438
1:2	48.0	403/437	48.2, 50.8	408/441
0:1	–	–	–	419/432

The APTMS semi-organic co-monomer was chosen to produce TEOS/APTMS–PCL hybrids because the acetate group resembles an ester linkage which might enhance organic/inorganic phase compatibility. However, simple visual inspection and ESEM suggest large-scale heterogeneity at lower APTMS concentrations. All films displayed opacity, but the degree of transparency increased as APTMS content increased. The TEOS/APTMS = 0:1 hybrid felt waxy and was the most transparent, possibly due to the least degree of microstructural heterogeneity. On the basis of handling, the films underwent a transition from brittle-to-rubbery (or waxy) as the APTMS content was increased and they display more mechanical integrity than the TEOS/PCL films.

APTMS is a strong semi-organic network modifier, in the sense of decreasing the average coordination number, and it is reasonable to think that less densely crosslinked ORMOSIL structures result with increasing APTMS concentration. The DSC scans for these hybrids (Fig. 7) also show no glass transition. The hybrids having 1:2 and

1:1 ORMOSIL compositions have dual, closely spaced, melting endotherms. T_m^{min} values are not significantly different than those for corresponding TEOS/DEDMS ratios, but the 1:0 (pure silicate, most rigid) composition was the most effective in retarding melting.

The TGA scans for these hybrids are shown in Fig. 8 and derived T_d values are in Table 2. The greatest T_d elevation relative to the PCL control was displayed by the TEOS/APTMS = 0:1 ORMOSIL composition. This hybrid, in fact, displayed the highest onset T_d of all the non-covalent films. For these, as for the TEOS/DEDMS–PCL films, the relative amount of organic material degraded was not as great as for the TEOS–PCL films. As with the TEOS and APTMS/TEOS compositions, the degradation profile is one, rather than two-step in nature.

While ORMOSIL compositions having other semi-organic co-monomers should be tested to establish a condition of generality, it appears that the first step random thermal scission of the middle of the chain is inhibited while the second step degradation that proceeds inward from the hydroxy-terminated chain ends is not.

3.4. Triethoxysilane-endcapped poly(ε-caprolactone)

The chemical structure of the triethoxysilane-endcapped PCL polymer that was created is shown in Fig. 1B. The synthesis was achieved after a period of 24–36 h. After the product was re-precipitated and filtered off, it was dried to remove residual solvent and moisture. The product was a fine white powder that was relatively stable under atmospheric conditions for a period of 1–2 weeks. After approximately 2 weeks, however, its solubility diminished, as it was no longer completely soluble in any of its previous solvents. Although portions of the sample did dissolve, complete dissolution was not possible, most likely due to crosslinking condensation reactions between the telechelic $-Si(OR)_3$ end groups in the presence of atmospheric moisture. Only then is the solvent able to dissolve the organic polymeric portion of the network, leaving the inorganic portion intact. However, in the initial 1–2 weeks, the product is completely soluble under atmospheric conditions.

GPC and MALDI-TOF MS were used to characterize polymer molecular weight after silane-endcapping. GPC data did in fact show a shift to higher molecular weight averages by an amount of about 330 g/mol, which closely corresponds to the molar weight of two triethoxysilane end groups. The MALDI-TOF mass spectra (not shown) were taken using the same experimental procedure as described earlier for the hydroxy-endcapped polymer. A main distribution was easily observed and peak-to-peak mass spacings of 114 were present, as before. However, a number of unexplained peaks appeared, most likely due to the polymer being in various states of alkoxysilane hydrolysis.

PCL polymers endcapped with the alkoxysilane functionality were also analyzed using FTIR and ^{13}C NMR spectroscopies, which indicated that the endcapping reactions did in fact occur.

The FTIR spectra (Fig. 3) for the reacted and unreacted polymers are almost identical, except for the signature peaks of modified end groups that are seen in two regions. These features appear weak as on the total spectrum because of the lower concentration of end groups relative to the total molecular weight of PCL.

Fig. 9 is an expansion of the spectrum shown in Fig. 3 for reacted PCL in the region 3700–3200 cm^{-1}. The RO–H stretching vibration of non-hydrogen bonded alcohol groups occurs in the range 3640–3610 cm^{-1} and this band shifts to lower wavenumbers (3600–3200 cm^{-1}) upon hydrogen bonding [50]. Moreover, these hydrogen bonded and non-hydrogen bonded peaks can be distinct from each other as opposed to being overlapped in a broad absorption envelope and distinct peaks are seen in this region for unreacted PCL. It is clear that both hydrogen bonded and non-hydrogen bonded RO–H groups are present. The spectrum for trialkoxysilane–telechelic PCL also shows these peaks with the following modifications. The band at ~3615 cm^{-1}, due to non-hydrogen RO–H groups, largely disappears while the band at ~3540 cm^{-1}, which is in the region for hydrogen bonded RO–H groups, is considerably diminished, while the band at ~3450 cm^{-1} is enhanced. This evidence points to a situation of greater hydrogen bonding on an ensemble average basis. There is also a shoulder on the high wavenumber side of the 3450 cm^{-1} peak, not seen in the spectrum for unreacted PCL, that is in the region of N–H stretching for non-hydrogen bonded secondary amines (3450–3310 cm^{-1}) [51]. If water is present, the IR analysis in this region would be problematic except for the fact that these films were carefully dried and there is no band at 1620 cm^{-1} which is the unambiguous signature of the water molecule. Thus, the IR evidence supports the claim of successful PCL end group reactions.

The other important spectral difference is the appearance

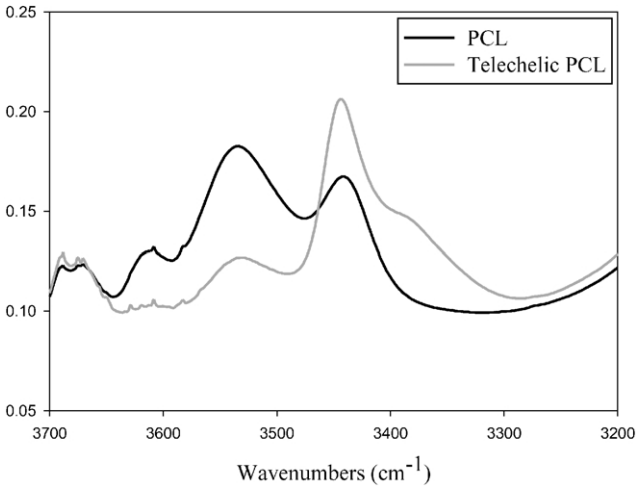

Fig. 9. Expansion of the spectrum in Fig. 3, in the region 3700–3200 cm^{-1}, for end group-reacted PCL.

of a peak at 1515 cm^{-1} which corresponds to the bending vibration in non-hydrogen bonded N–H groups in secondary amines (1580–1490 cm^{-1}) [51]. The appearance of this peak results from the interaction between the N–H bending vibration and the C–N stretching vibration.

In addition, a very slight shift to longer wavelength was observed in the carbonyl peak (1700 cm^{-1}), which might be due to a lowered relative number of ester to urethane C=O groups.

Finally, there is a peak at around 1100 cm^{-1} on both spectra as shown in Fig. 3 that is due to PCL. A shoulder is seen on the right side of this peak for triethoxysilane-endcapped PCL, but not for OH-terminated PCL. This peak is in the region of the Si–OR bond stretching vibration, a signature of the intended end group [52].

The ^{13}C NMR spectrum of the silane-endcapped polymer reinforces these findings. The representative peaks of the PCL backbone appear in the spectrum of the final product along with those of ICPTES. The ^{13}C NMR spectrum of the silane-endcapped product shows no isocyanate carbons ($\delta = 125$ ppm), but does show the peak for the carbonyl carbon of the urethane linkage ($\delta = 159$ ppm). This peak is too small to see in the full spectrum, but the region has been expanded in the inset in Fig. 4. This peak, labeled 'b', is separate from that for the internal carbonyl carbons along the chain. Another indication of the success of this reaction is the disappearance of peaks representing the methylene carbons adjacent to the alcohol end groups (ε^{OH} at -62 ppm and δ^{OH} at -32 ppm) as identified in Fig. 4, of the hydroxy-telechelic polymer.

The peak at 20 ppm and those between 120 and 140 ppm represent the methyl and aromatic groups, respectively, of the residual toluene in the sample because the sample was removed for analysis before completely drying. The sample was taken before complete drying because the alkoxysilane groups are reactive, and it was thought that they would react fairly quickly upon drying. The triplet at 77 ppm is from the deuterated solvent used (chloroform). The peak at 50 ppm represents residual methanol, which was used to re-precipitate the solid product. This appears, as does the toluene, because the sample was not completely dry before characterization.

3.5. Telechelic poly(ε-caprolactone) film formation

Telechelic PCL film formation was successfully achieved via sol–gel processing by mixing the triethoxysilane-endcapped PCL material with 5 wt% TEOS. ESEM micrographs of these films show surfaces that are smooth and homogeneous on the scale of tens-of-microns. Films displayed very good strength on handling and visible inspection revealed no phase separation or gross defects that would scatter light. Color-wise, the films were slightly yellow and translucent, although not totally transparent. As stated in Section 2, this film was formed without the use of a semi-organic co-monomer and no pre-measured water was added (atmospheric water, under ambient laboratory conditions was sufficient) or the usual sol–gel reaction catalysts, such as an acid. In the liquid state, the triethoxysilane–telechelic polymer is very reactive and forms a network within a period of a few hours.

The DSC thermogram for this telechelic material and that for unmodified hydroxy-endcapped PCL is shown in Fig. 10. The glass transition for each is only slightly evident on the top plot but is more clearly seen on the expanded scale in the bottom plot. T_g significantly increases from -63 °C for the hydroxy-telechelic PCL polymer to -53 °C for the reacted triethoxysilane–telechelic polymer. It is reasonable that this increase in T_g results from the formation of covalent coupling, by the formation of Si–O–Si links via condensation reactions, between the organic and TEOS-derived silicate phases. The anchoring of chain ends in this way would restrict PCL chain mobility so that a higher temperature is required for activation. The non-covalent films did not shown this behavior, presumably because the polymer was not as strongly bound to the TEOS-derived

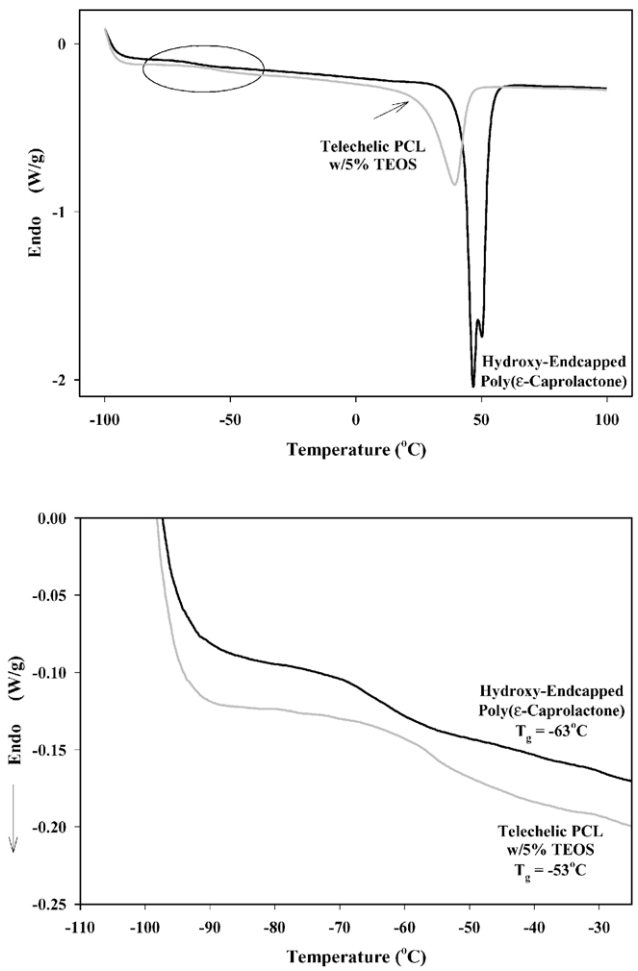

Fig. 10. DSC second heating scans of hydroxy- and triethoxysilane-endcapped + TEOS-treated PCL (top), and enlarged DSC scans for the same in the glass transition region (bottom).

Table 3
O_2 permeability (P), diffusivity (D), and solubility (S) coefficients for hydroxy- and silane-endcapped PCL

Sample	P cm^3(STP)cm/m^2/atm/day	D m^2/s	S cm^3(STP)/cm^3/atm
PCL	0.818	23.4	0.041
Telechelic PCL with 5% TEOS	0.566	16.2	0.042
PET	0.469	5.60	0.098

silicate component and the end groups were not tethered in this way.

The magnitude of the melting transition decreases upon inorganic modification, as also noted for the previous hybrid films, except that here the effect is dramatic. Because the vertical scale for the thermograms is reduced to a per-gram-of-polymer component basis, this represents a genuine suppression of melting. T_m^{min} decreased by 8 °C relative to pure PCL and the dual peak behavior disappears. This fact, combined with the lowered degree of crystallinity relative to pure PCL, as well as the fact that chain motions in the amorphous regions are more restricted, might indicate that smaller, more poorly developed crystallites form under the influence of the constraints posed by the inorganic modification. It is presumed that this restricted chain mobility is caused by a tethering of PCL chains, at either or both ends, to the silicate phase. Of course, these silicate regions can also simply act as simple volume-filling obstacles to crystal growth that occurs in a complex process that is simultaneous with the growth of silicate particles during the complex film formation.

The TGA thermogram for the TEOS-modified alkoxysilane–telechelic material is shown in Fig. 11. While this hybrid does not display strong two-step behavior, there is a weak inflection point at approximately the temperature as that which defines the high temperature event for the hydroxy-telechelic sample. Given that the onset of mass loss has been retarded, it might be concluded that this modification has affected both high and low temperature degradation mechanisms. There is an increase of 30 °C in overall T_d in the thermogram of the TEOS-modified

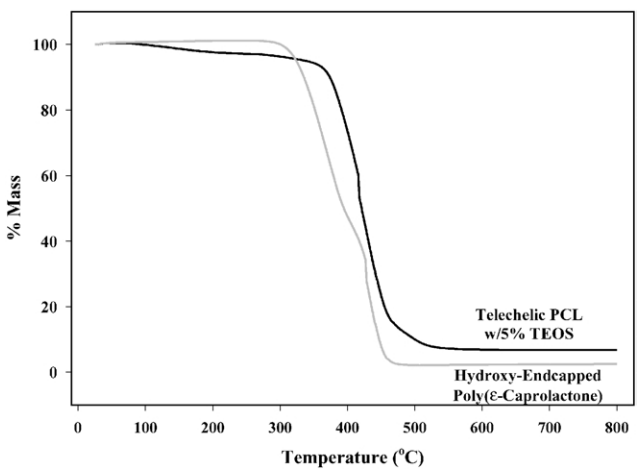

Fig. 11. TGA scans for hydroxy- and triethoxysilane-endcapped PCL.

alkoxysilane–telechelic material, which is less than that observed for the non-covalent materials. However, the non-covalent materials contain considerably more of an inorganic component. Thus, it is significant that the 95%, by mass, of the PCL component is significantly influenced by the small fraction of the inorganic phase. Of course, it is also possible that the restriction of PCL chain mobility, in addition to the removal of the hydroxyl end groups, will contribute to retarding thermal degradation.

3.6. O_2 permeation

Samples of PCL and telechelic PCL modified with 5% TEOS were quenched in cold water and compression molded into 25 mil (0.635 mm) thick amorphous plaques, which were then tested for O_2 permeation. This particular hybrid was chosen on the basis of its mechanical integrity. The derived, P, D and S values are listed in Table 3. Owing to the fact that these hybrids were of interest primarily within the realm of packaging materials, data was also collected for a sample made from standard poly(ethylene terephthalate) (PET) bottle resin as a reference. It can be seen that the incorporation of 5 wt% TEOS results in a 30% reduction in oxygen permeation. It is interesting that the physical mixing of the same weight percent (5 wt%) of microtalc into PET also decreases oxygen permeability by 30% [42]. Incorporation of 5% talc into PET decreased O_2 solubility by only 5%, but decreased O_2 diffusivity by ~25%. The decrease in O_2 permeation observed upon incorporation of 5% TEOS in our materials results entirely from a reduction in diffusivity while the oxygen solubility is unchanged. The shift in diffusion kinetics can be rationalized in a general way in terms of polymer chain dynamics and tortuosity within this heterogeneous organic/inorganic material.

It has been well established that the solubility of O_2 in PET-based systems can be explained in terms of static free volume, which is proportional to the difference between polymer T_g and the experimental temperature [53–56]. O_2 diffusivity in PET has similarly been demonstrated to result from dynamic free volume, which correlates with segmental motions in the amorphous phase, which are related to the sub-T_g, γ-relaxation. However, while both PET and PCL are polyesters, the amorphous phase in the latter is above the glass transition, while the former is not, at room temperature.

4. Conclusions

Organic–inorganic hybrid materials were synthesized based on sol–gel polymerizations for TEOS or/and organoalkoxysilane monomers in the presence of PCL. The molecular weights and chemical structures of these hybrids were determined by the use of GPC, MALDI-TOF mass spectrometry, and ^{13}C NMR and FTIR spectroscopic methods.

Non-covalent silicate–PCL and ORMOSIL–PCL hybrids were studied by DSC. The rather constant value of T_g for the PCL phase in the silicate–PCL hybrids implies poor organic/inorganic component mixing. However, PCL phase melting endotherms did vary with silicate content. These endotherms were of a dual peak nature, which suggests the existence of two different crystal structures. TGA analyses of these non-covalent films revealed a significant elevation of the degradation onset temperature of PCL caused by the incorporation of a silicate component in this way. It appears that the first degradation step involving random scission throughout the middle of the chain is inhibited while the second step, that proceeds inward from the hydroxy-terminated chain ends, is not affected.

No PCL glass transition is evident for the ORMOSIL–PCL hybrids, where DEDMS is the semi-organic co-monomer and melting is not of a two-step nature as in the previous case. Moreover, there are significant increases in T_d relative to pure PCL. ORMOSIL–PCL hybrids where APTMS is the semi-organic co-monomer do not exhibit a glass transition and have dual, closely spaced melting endotherms.

Triethoxysilane-endcapped PCL was successfully synthesized and its chemical structure was verified by GPC, MALDI-TOF mass spectrometry, and FTIR and NMR spectroscopies. When this form was reacted with a small fraction (5%) of TEOS, there was a significant improvement over pure PCL and non-covalent hybrid films in having a morphologically uniform surface. A glass transition is present on second DSC scans, but T_g significantly increases from $-63\,^{\circ}C$ for the hydroxy-telechelic PCL polymer to $-53\,^{\circ}C$ for the TEOS-reacted triethoxysilane–telechelic polymer. This T_g increase likely results from Si–O–Si bond formation that links the PCL and silicate phases through the end groups. Non-covalent [TEOS and ORMOSIL]–PCL films did not show this behavior. Melting transition magnitude decreased upon inorganic modification, although T_m^{min} decreased by $8\,^{\circ}C$ relative to pure PCL, and it is suggested that smaller, more poorly developed crystallites form under chain-restrictive conditions. TGA scans show appreciable increase in T_d relative to the control. Both the high and low temperature degradation processes appear to be affected by the inorganic modification.

The silane–telechelic PCL films have an oxygen permeability that is less than that of pure PCL films by 30%. This is totally attributed to a decrease in diffusion coefficient with practically no change in solubility coefficient.

Future work will focus on affecting increased phase compatibility and a compositional optimization of silane–telechelic PCL-based systems with regard to mechanical, thermal, optical, and molecular transport properties. Also, studies of the hydrolytic and microbial degradation of these materials will be conducted within the context of biodegradable materials.

Acknowledgements

Funding for the PerSeptive Biosystems Voyager-RP Biospectrometry Workstation was provided through the Defense University Research Instrumentation Program (DURIP), Grant DAAG55-97-1-0067. Financial support was provided by KoSa to both the University of Southern Mississippi and Case Western Reserve University. Support is also acknowledged from the State of Mississippi National Science Foundation EPSCoR programs, Grants EPS-9452857 and EPS-0083128.

References

[1] Brinker CJ, Scherer GW. Sol–gel science: the physics and chemistry of sol–gel processing. Boston: Academic Press; 1990.
[2] Brinker CJ, Scherer GW. J Non-Cryst Solids 1985;70:301.
[3] Keefer KD. Silicon based polymer science: a comprehensive resource. American Chemical Society Advances in Chemistry Series No. 224, Washington, DC: American Chemical Society; 1984.
[4] Hench LL, West JK. Chem Rev 1990;90:33.
[5] Yoldas BE. J Non-Cryst Solids 1984;63:145.
[6] Schmidt H, Wolter H. J Non-Cryst Solids 1990;121:428.
[7] Landry CJT, Coltrain BK, Teegarden DM, Long TE, Long VA. Macromolecules 1996;29:4712.
[8] Coltrain BK, Landry CJT, O'Reilly JM, Chamberlain AM, Rakes GA, Sedita JS, Kelts LW, Landry MR, Long VK. Chem Mater 1993;5:1445.
[9] Mauritz KA, Ju R. Chem Mater 1994;6:2269.
[10] Novak BM, Ellsworth MW, Verrier C. Hybrid organic–inorganic composites. American Chemical Society Symposium Series 585, Washington, DC: American Chemical Society; 1994. Chapter 8.
[11] Sperling LH. Interpenetrating polymer networks and related materials. New York: Plenum Press; 1981. Chapter 1.
[12] Odian G. Principles of polymerization. New York: Wiley; 1991. chapter 2.
[13] Tian D, Dubois P, Jerome R. Polymer 1996;37(17):3983.
[14] See articles throughout Chemistry Materials 2001;13(10).
[15] Sanchez C, Ribot F. New J Chem 1994;18:1007.
[16] Phillip G, Schmidt H. J Non-Cryst Solids 1984;63:283.
[17] Wilkes GL, Orler B, Huang HH. Am Chem Soc Polym Prepr 1985;26(2):300.
[18] Huang HH, Orler B, Wilkes GL. Macromolecules 1987;20:1322.
[19] Huang HH, Orler B, Wilkes GL. Polym Bull 1985;14:557.
[20] Sur G-S, Mark JE. Eur Polym J 1985;21(12):1051.
[21] Huang HH, Wilkes GL, Carlson JG. Polymer 1989;30:2001.
[22] Tian D, Blatcher S, Dubois Ph, Jerome R. Polymer 1997;397(4):855.
[23] Persenaire O, Alexandre M, Degee P, Dubois P. Biomacromolecules 2001;2:288.

[24] Potts JE, Clendenning RA, Ackart WB, Neigisch WD. In: Guillet J, editor. Polymer science and technology, vol. 3. New York: Plenum Press; 1973. p. 61–80.
[25] Tokiwa Y, Ando T, Suzuki T. J Ferment Technol 1976;54:603.
[26] Kavelman R, Kendrick B. Mycologia 1978;70:87.
[27] Fields RD, Rodriguez F, Finn RK. J Appl Polym Sci 1974;18:3571.
[28] Benedict CV, Cook WJ, Jarrett P, Cameron JA, Huang SJ, Bell JP. J Appl Polym Sci 1983;28:327.
[29] Schindler A, Jeffcoat AR, Kimmel GL, Pitt CG, Wall ME, Zweidinger RA. In: Pearce EM, Schaefgen RJ, editors. Contemporary topics in polymer science, vol. 2. New York: Plenum Press; 1977.
[30] Mayer JM, Kaplan DL. Trends Polym Sci 1994;2(7):227.
[31] Union Carbide TONE® Polymer Product Literature; 1988.
[32] Deng Q, Moore RB, Mauritz KA. Chem Mater 1995;7:2259.
[33] Deng Q, Cable KM, Moore RB, Mauritz KA. J Polym Sci, Part B: Polym Phys Ed 1996;34:1917.
[34] Deng Q, Hu Y, Moore RB, McCormick CL, Mauritz KA. Chem Mater 1997;9:36.
[35] Young SK, Mauritz KA. J Polym Sci, Part B: Polym Phys 2001; 39(12):1282.
[36] Mountz DA, Reuschle DA, Mauritz KA. ACS Polym Prepr 1999; 40(2):713.
[37] Sherman JW. PhD Dissertation. School of Polymers and High Performance Materials, The University of Southern Mississippi; 2000.
[38] Storey RF, Hickey TP. J Polym Sci, Part A: Polym Chem 1993;31: 1825.
[39] Silverstein RM, Bassler GC, Morrill TC. Spectrometric identification of organic compounds. New York: Wiley; 1991. Chapter 3.
[40] Conley RT. Infrared spectroscopy. Boston: Allyn and Bacon, Inc; 1972. chapter 5.
[41] Pouchert CJ. The Aldrich Library of infrared spectra, 3rd ed. Aldrich Chemical Company, Inc; 1981.
[42] Sekelik DJ, Stephanov E, Nazarenko S, Schiraldi DA, Hiltner A, Baer E. J Polym Sci, Part B: Polym Phys 1999;37:847.
[43] Liu RYF, Schiraldi DA, Hiltner A, Baer E. J Polym Sci, Part B: Polym Phys 2002;40:862.
[44] Polyakova A, Stepanov EV, Sekelik D, Schiraldi DA, Hiltner A, Baer E. J Polym Sci, Part B: Polym Phys 2001;39:1911.
[45] Storey RF, Taylor AE. J Macromol Sci, Pure Appl Chem 1998; A35(5):723.
[46] Siuzdak DA, Start PR, Mauritz KA. J Appl Polym Sci 2000;77:2832.
[47] Lambert AA, Mauritz KA, Schiraldi DA. J Appl Polym Sci 2002;84: 1749.
[48] Babonneau F, Thorne K, Mackenzie JD. Chem Mater 1989;1:554.
[49] Deng Q, Jarrett W, Moore RB, Mauritz KA. J Sol–Gel Sci Technol 1996;7:185.
[50] Conley RT. Infrared spectroscopy. Boston: Allyn and Bacon, Inc; 1972. p. 129–32.
[51] Conley RT. Infrared spectroscopy. Boston: Allyn and Bacon, Inc; 1972. p. 147.
[52] Juangvanich N, Mauritz KA. J Appl Polym Sci 1998;67:1799.
[53] Polyakova A. PhD Dissertation. Department of Macromolecular Science, Case Western Reserve University; 2000.
[54] Polyakova A, Schiraldi DA, Hiltner A, Baer E. J Polym Sci, Part B: Polym Phys 2001;39:1889.
[55] Querishi N, Stepanov EV, Schiraldi DA, Hiltner A, Baer E. J Polym Sci, Part B: Polym Phys 2000;38:1679.
[56] Polyakova A, Stephanov EV, Sekelik D, Schiraldi DA, Hiltner A, Baer E. J Polym Sci, Part B: Polym Phys 2001;39:1911.